Published in final edited form as:
Immunity. 2008 October 17; 29(4): 602–614. doi:10.1016/j.immuni.2008.07.015.

Imaging of Effector Memory T Cells during a Delayed-Type Hypersensitivity Reaction and Suppression by Kv1.3 Channel Block

Melanie P. Matheu[1,6], **Christine Beeton**[1,6], **Adriana Garcia**[1], **Victor Chi**[1], **Srikant Rangaraju**[1], **Olga Safrina**[1], **Kevin Monaghan**[1], **Marc I. Uemura**[1], **Dan Li**[2], **Sukumar Pal**[2], **Luis M. de la Maza**[2], **Edwin Monuki**[2], **Alexander Flügel**[3], **Michael W. Pennington**[4], **Ian Parker**[1,5], **K. George Chandy**[1,7], and **Michael D. Cahalan**[1,7,*]

[1]Department of Physiology and Biophysics and the Center for Immunology, University of California, Irvine, Irvine, CA 92697-4561, USA

[2]Department of Pathology, University of California, Irvine, Irvine, CA 92697, USA

[3]Department of Neuroimmunology, Max-Planck-Institute of Neurobiology, 82152 Martinsried, Germany

[4]Bachem Bioscience Inc., King of Prussia, PA 19406, USA

[5]Department of Neurobiology and Behavior, University of California, Irvine, Irvine, CA 92697, USA

SUMMARY

Effector memory T (Tem) cells are essential mediators of autoimmune disease and delayed-type hypersensitivity (DTH), a convenient model for two-photon imaging of Tem cell participation in an inflammatory response. Shortly (3 hr) after entry into antigen-primed ear tissue, Tem cells stably attached to antigen-bearing antigen-presenting cells (APCs). After 24 hr, enlarged Tem cells were highly motile along collagen fibers and continued to migrate rapidly for 18 hr. Tem cells rely on voltage-gated Kv1.3 potassium channels to regulate calcium signaling. ShK-186, a specific Kv1.3 blocker, inhibited DTH and suppressed Tem cell enlargement and motility in inflamed tissue but had no effect on homing to or motility in lymph nodes of naive and central memory T (Tcm) cells. ShK-186 effectively treated disease in a rat model of multiple sclerosis. These results demonstrate a requirement for Kv1.3 channels in Tem cells during an inflammatory immune response in peripheral tissues. Targeting Kv1.3 allows for effector memory responses to be suppressed while central memory responses remain intact.

INTRODUCTION

Costimulation-independent $CCR7^{-}CD45RA^{-}$ effector memory T (Tem) cells are essential mediators of numerous chronic inflammatory autoimmune diseases including rheumatoid arthritis (RA), multiple sclerosis (MS), type I diabetes mellitus (T1DM), and psoriasis (Beeton et al., 2006; Conrad et al., 2007; Ellis and Krueger, 2001; Haegele et al., 2007; Kivisakk et al.,

*Correspondence: mcahalan@uci.edu.
[6]These authors contributed equally to this work
[7]These authors contributed equally to this work

SUPPLEMENTAL DATA

Supplemental Data include Supplemental Experimental Procedures, one table, seven figures, and thirteen movies and can be found with this article online at http://www.immunity.com/cgi/content/full/29/4/▪▪▪/DC1/.

2004; Krakauer et al., 2006; Rus et al., 2005; Wulff et al., 2003b). Tem cells are a tissue-resident subset of memory T cells that display immediate effector function at the site of antigen deposition (Sallusto et al., 2004). Tem cells respond in nonlymphoid tissues, where they initiate a localized inflammatory immune response. Upon activation, $CD4^+$ Tem cells give rise to T helper 1 cells (Tem effectors) that produce interferon gamma (IFN-γ), interleukin-2 (IL2), tumor necrosis factor alpha and beta (TNF-α and TNF-β), all potent mediators of the inflammatory response that recruit and activate macrophages, which, in turn, secrete TNF-α and interleukin-1 (IL1). Together, these events inaugurate the self-propagating localized inflammatory immune response that is typical of delayed-type hypersensitivity (DTH) and autoimmune diseases. DTH in rats, as in humans, is characterized by tissue swelling and infiltration in the subcutaneous layer and dermis by IFN-γ-and TNF-α-expressing Tem cells (Gaga et al., 1991; Hancock et al., 1994).

Fluorescence microscopy and single-cell patch-clamp studies show that quiescent human peripheral blood $CD4^+$ and $CD8^+$ naive, central memory T (Tcm), and Tem cells have similar channel phenotypes expressing ~300 voltage-gated Kv1.3 potassium channels per cell and ~10 calcium-activated KCa3.1 potassium channels per cell. Upon activation, naive and Tcm cells upregulate KCa3.1 channels, whereas Tem cells upregulate Kv1.3 channels when they change into Tem effectors (Wulff et al., 2003b). In Tem cells, Kv1.3 localizes at the immune synapse during antigen presentation and regulates the membrane potential of these cells, maintaining the driving force for influx of Ca^{2+} ions during cell activation (Beeton et al., 2005; Chandy et al., 2004; Panyi et al., 2004; Rus et al., 2005). Genetic silencing of Kv1.3 in human T cells leads to an expansion of Tcm cells and a depletion of Tem cells, highlighting the functional importance of the Kv1.3 channel in the Tem population (Hu et al., 2007). Specific Kv1.3 inhibitors preferentially suppress calcium flux, cytokine production, and proliferation in vitro of $CCR7^-$ Tem effector cells without affecting the function of naive and Tcm cells (Beeton et al., 2005; Beeton et al., 2006; Wulff et al., 2003b).

Disease-associated autoreactive T cells from the blood of patients with MS, RA, or T1DM display the Tem-effector-specific phenotype of $Kv1.3^{hi}$ in the blood, whereas T cells specific for disease-irrelevant antigens from the same patient populations or T cells specific for autoantigens in control populations are $CCR7^+Kv1.3^{lo}$ naive T or Tcm cells (Beeton et al., 2006; Rus et al., 2005; Wulff et al., 2003b). In rats, T cells at the site of a DTH response are $CD4^+CCR7^-CD45RC^-Kv1.3^{hi}$ Tem effector cells (Beeton et al., 2006), and the T cells infiltrating the skin in acute contact dermatitis are $CD8^+CCR7^-CD45RC^-TKv1.3^{hi}$ Tem effector cells (Azam et al., 2007). Thus, T cells at sites of inflammation in humans and in rats are $Kv1.3^{hi}$ Tem effectors.

The differences in K^+ channel phenotype between naive, Tcm cells, and Tem cells, together with the selective suppressive effects of Kv1.3 inhibitors on Tem cells, make Kv1.3 an attractive therapeutic target, with potential to spare chronic autoimmune-disease sufferers from side effects associated with broad-range immunosuppression. Specific inhibitors of Kv1.3 suppress active DTH and contact dermatitis, both caused by skin-homing Tem cells (Azam et al., 2007; Beeton et al., 2006; Soler et al., 2003), and have pronounced effects on adoptive experimental autoimmune encephalomyelitis (EAE), pristane-induced arthritis, and experimental autoimmune diabetes mellitus, common models for MS, RA, and T1DM, respectively (Beeton et al., 2005; Beeton et al., 2006). Moreover, these inhibitors demonstrate good safety profiles in both rats and Rhesus macaques (Azam et al., 2007; Beeton et al., 2006; Pereira et al., 2007).

Here, by two-photon imaging of ear tissue during a DTH response, we provide direct visualization of Tem cell dynamics and resolve the in vivo implications of Kv1.3 channel block in an antigen-challenged Tem cell population. Adoptive transfer of in vitro-activated GFP-

expressing ovalbumin-specific $CD4^+CCR7^-CD45RC^-Kv1.3^{hi}$ Tem cells induces a highly reproducible DTH response upon subsequent local challenge by subcutaneous injection of antigen. By combining this system with two-photon microscopy and peripheral tissue preparation for live-cell imaging, we imaged the activation and motility of Tem cells in inflamed tissue during a DTH reaction. In addition, we show that ShK-186 preferentially suppresses the in vivo motility and activation of Tem cells at the inflamed site without affecting the motility of naive and Tcm cells in lymph nodes. Therefore, we examined whether the selective suppression of Tem cells via Kv1.3 blockade effectively treats chronic EAE, a model of MS, and whether such therapy compromises the immune response to two common and medically important infectious agents—influenza virus and *Chlamydia trachomatis*.

RESULTS

GFP^+ Ovalbumin-Specific T Cells Display Tem Markers and Abundant Kv1.3 Channels

Ova-specific GFP^+ $CD4^+$ rat Tem cells (Flugel et al., 1999) lack surface expression of CCR7 and CD45RC (Figure 1A) and upon in vitro activation upregulate Kv1.3 expression (Figure 1B and Figure S1A, available online). These cells also upregulate Kv1.3 channels in vivo during the DTH response (Figure 1C). Kv1.3 numbers in GFP^+ Ova-specific Tem cells were low 3 hr after Ova challenge in the ear, indicating that these cells had reverted to a quiescent state during the 48 hr following adoptive transfer. As DTH progressed, the cells reactivated in the ear and expressed large numbers of Kv1.3 channels 24 hr after Ova challenge. CD25 and VLA-1 were also upregulated, whereas expression of VLA-4α (CD49d) was downregulated and expression of CD11a and CD29 was unchanged (Figure S1B).

Development of Adoptive DTH and Preparation of Tissue for Imaging

Ova-specific GFP^+ Tem effector cells generated by antigen-specific activation in vitro were adoptively transferred intraperitoneally into Lewis rats that were subsequently challenged in one ear with ovalbumin conjugated to Texas red (Ova-TR) and in the other ear with saline (Figure S2). Substantial increases in ear thickness (>50% increase in thickness) were seen as early as 3 hr after antigen challenge (Figure 2A). The increase in ear thickness was maintained through the 42 hr time point. Using an ear explant preparation, we removed the epidermis and some of the dermis along with hair follicles (Figure 2B) that produced image-obscuring autofluorescence. Extravascular cells were imaged in the remaining dermis and underlying subcutaneous tissue (Figure 2C).

Motility of Tem Cells and Tem Effectors during Development of DTH

Two-photon imaging (Figure 3A–3C and Movie S1) revealed Ova-specific GFP^+ Tem cells (green), presumptive (antigen-presenting cells (APCs) that had taken up and concentrated Ova-TR (red), and collagen structures visualized with second-harmonic generation (blue). At the 3 hr time point after Ova-TR injection into the ear, the majority of GFP^+ Ova-specific cells were immotile and usually maintained stable contact with red-labeled Ova-TR-bearing APCs (Figure 3A and Movie S2). At the 24 hr time point, enlarged and highly motile cells extended long membrane projections while migrating along collagen in distinct subcutaneous regions and paused but did not arrest on Ova-TR-bearing APCs (Figure 3B and Movie S3). The heterogenous localization of Tem effector cells was confirmed histologically (data not shown) and is consistent with previous histological studies of DTH in rats and humans (Gaga et al., 1991; Hancock et al., 1994). At the 42 hr time point, effectors remained enlarged and highly motile (Figure 5D) and continued to crawl along collagen-fiber bundles in the midst of Ova-TR-containing APCs (Figure 3C and Movie S4).

At the 3 hr time point, effector cells in contact with a local APC migrated with an average velocity of 3.9 μm/min, slower than cells in contact with collagen (5.3 μm/min) (Figure 3D).

As DTH progressed, enlarged Tem cells migrated faster, with average velocities at 24 hr of 7.4 μm/min when in contact with APCs and 11.1 μm/min when in contact with collagen (Figure 3E). By 42 hr, the enlarged effectors maintained high velocities, moving at 7.0 μm/min when making short-lived contacts with APCs and 12.0 μm/min while crawling along collagen (Figure 3F). Interestingly, the size of the activated effectors correlated with their velocity; larger cells moved with higher average velocities than smaller cells (Figure 3G). At the 3 hr time point, ~70% of cells were in contact with Ova-TR-bearing APCs at any given time and, as the DTH reaction developed, the proportion of time that effector T cells were in contact with APCs decreased progressively (Figure 3H). Contact durations at 3 hr often exceeded the length of our imaging records (~30 min). Later in the DTH reaction, interaction times became progressively shorter, with mean durations of 7 min at 24 hr and 3 min at 42 hr (Figure 3I).

In order to confirm that cell motility and contact durations in the ear tissue were not significantly altered by the explant imaging preparation, we performed intravital imaging of adoptive DTH in the rat paw 24 hr after antigen challenge (Figure S3 and Movie S5). Velocities (averaging 8.5 μm/min) and the average contact duration (7 min) of enlarged, activated Ova-specific GFP^+ T cells in the rat paw were similar to those characteristics determined by imaging of ear tissue.

In addition, to examine the behavior of bystander T cells, we imaged motility of Ova-specific GFP^+ T cells during a DTH response to an irrelevant antigen. After initiation of an active DTH response with hen-egg lysozyme (HEL), Ova-specific Tem effector cells infiltrated the inflamed ear tissue and migrated rapidly along collagen fibers with an average velocity of 10.4 um/min (Figure 3J–3L; Movie S6), comparable to the velocities of antigen-activated Tem cells migrating on collagen (Figure 3B and 3E). Unlike Tem cell behavior in the DTH response to cognate antigen, Tem cells infiltrating the site of inflammation induced by irrelevant antigen failed to enlarge (Figure 3L), indicating that they did not reactivate in vivo.

Tem Effector Cell Movement along Collagen

We further analyzed the patterns of migration of highly motile Tem effector cells along collagen networks in inflamed tissue (24 hr time point) as they moved along collagen fibers and interacted with Ova-TR-bearing APCs (Figure 4). Effector T cells predominantly followed paths parallel to the larger collagen bundles, (white cell tracks, Figure 4A and 4B; Movie S7). Although occasional cells crossed the collagen bundles, the overall displacement from origin/distance traveled (meander index) was consistent with movement directed by structural constraints (Figure 4C). At junctions within the local collagen scaffold, effector cells closely tracked along the collagen, often resulting in circuitous pathways in which the overall cell displacement was minimal (Figure 4D and Movie S8). Effectors were also able to change direction by traversing from fiber to fiber at junctions (red and gold tracks; Figure 4E). This pattern of directed migration of Tem effectors predominantly along collagen bundles contrasts sharply with the apparent random-walk migration of $CCR7^+$ T cells in rat (cf. Figure 7D) or mouse lymph nodes (Miller et al., 2002).

Suppression of DTH by Kv1.3 Channel Block

ShK-186, a synthetic analog of the ShK peptide isolated from the sea anenome *Stichodactyla helianthus*, is modified at the N terminus to increase specificity for Kv1.3 while retaining picomolar potency (Beeton et al., 2005, 2006). ShK-186 blocked the Kv1.3 current in the Ova-specific GFP^+ Tem cells in a dose-dependent manner (Figure 5A). At concentrations that blocked the Kv1.3 channel, ShK-186 suppressed antigen-specific proliferation of the Tem cells (Figure 5B). ShK-186 (100 mg/kg) administered by subcutaneous injection in the scruff of the neck at the time of Ova-TR challenge and 24 hr later (Figure S4A) reduced DTH (smaller D ear thickness) at all time points compared to rats given saline injections (Figure 5C). The

circulating levels of ShK-186 in injected rats (Figure S4B) were sufficient to suppress the proliferation of the Tem cells. The total number of extravascular GFP^+ Tem effectors recovered from each ear was the same in rats administered saline or ShK-186 injections (Figure 5D), indicating that ShK-186 treatment did not prevent Ova-specific GFP^+ Tem effectors from entering the ear tissue. By 42 hr the numbers of GFP^+ cells in the ear had decreased in both saline-and ShK-186-treated rats (Figure 5D).

Suppression of Tem Cell Motility and Activation by Kv1.3 Channel Block

At all time points after Ova-TR injection into the ear, the majority of GFP^+ Ova-specific Tem cells in ShK-186-treated rats were in contact only with the collagen matrix (Figure 6A–6C and 6G; Movie S9) and only made intermittent contacts with Ova-TR-bearing APCs, in contrast to saline-treated animals, in which Tem cells maintained stable contact with APCs. At 24 and 42 hr into the DTH reaction, the Tem cells remained small and relatively immotile in ShK-186-treated rats (Figure 6B and 6C; Movie S10 and Movie S11). Mean velocities at 3 hr, 24 hr, and 42 hr in ShK-186-treated rats were < 2.5 μm/min (Figure 6D–6F), in striking contrast to the rapid velocities (7–12 μm/min) seen in saline-treated control rats at later times (Figure 3E and 3F). Moreover, Tem cells failed to enlarge during the course of the DTH reaction (Figure 6H). These results indicate that, although Ova-specific Tem cells enter normally into inflamed tissues in ShK-186-treated rats, once in the tissue the peptide prevents the cells from becoming reactivated and immobilizes them.

Skin-homing memory T cells involved in DTH express high levels of b1 integrins that facilitate the migration of these cells to a site of antigenic challenge via integrin interaction with matrix proteins (Andreasen et al., 2003; Ferguson et al., 1991; Mackay et al., 1992; Picker et al., 1990). To identify a mechanism that may underlie ShK-186's activity, we examined the peptide's effect on activated b1 integrin expression in Ova-specific Tem cells. Activation of b1 integrin in T cells is calcium dependent and is probably mediated by a concerted mechanism involving the increase of intracellular calcium and activation of PKC (Lim et al., 2000; Rowin et al., 1998). We have previously shown that ShK-186 treatment suppresses antigen-induced calcium signaling in Tem cells (Beeton et al., 2006). Therefore, we hypothesized that ShK-186 treatment immobilized Tem cells at the site of DTH by reducing intracellular calcium and thereby inhibiting the activation of β1 integrin. To mimic the conditions of the in vivo experiments, we incubated Ova-specific Tem cells in vitro with antigen-pulsed irradiated thymocytes for 48 hr to generate activated Tem effectors. In other experiments, Tem cells were ''rested'' in IL2-containing medium for 6 days (resting Tem cells). Intracellular calcium and activated b1 integrin expression were then measured in activated or resting Tem cells exposed to 100 nM ShK-186 or vehicle for 30 min. As expected, intracellular calcium was elevated in activated Tem effectors, compared to resting Tem cells (Figure S5). Acute exposure to ShK-186 significantly lowered intracellular calcium in activated Tem cells ($p < 10^{-6}$), but did not affect intracellular calcium in resting Tem cells. We also measured activated β1 integrin expression by staining with the HUTS-21 mAb (Luque et al., 1996) and gating on the GFP^+ population. HUTS-21 staining was detected on activated but not resting Tem cells (Figure 6I and 6J). ShK-186 reproducibly minimized HUTS-21 staining in activated Tem cells to levels comparable to background staining ($p < 0.01$), paralleling its inhibitory effect on intracellular calcium. Confirming the calcium dependence of β1-integrin activation, acute removal of external Ca^{2+} brought HUTS-21 expression to baseline ($p < 0.01$). Our results thus suggest that ShK-186 immobilizes Tem cells at inflammatory sites by suppressing calcium signaling and thereby preventing β1 integrin activation.

Motility of $CCR7^+$ T Cells in the Lymph Node Is Unaltered by ShK-186 Treatment

The finding that ShK-186 dramatically reduces motility of Tem cells in ear tissue prompted us determine its effects on resting T cells in lymph node. A pool of predominantly

$CD3^+CCR7^+$ cells (Figure 7A) was purified from secondary lymphoid organs, labeled with CFSE, and transferred into Lewis rats, which received either ShK-186 or saline by subcutaneous injection at the time of cell transfer. CFSE-labeled T cells in both groups (saline or ShK-186-treated rats) were highly motile, displaying no difference in cell localization velocities, directional preference, or meander index within the lymph node (Figure 7B–7F; Movie S12 and Movie S13). Thus, ShK-186 does not affect the motility of lymph-node-resident T cells.

Evaluation of ShK-186 in Other Disease Models

We evaluated the therapeutic effectiveness of ShK-186 in a rat EAE model that closely follows the clinical course of human MS. DA rats immunized with spinal cord homogenate and complete Freund's adjuvant developed relapsing-remitting EAE about 10 days after immunization (Figure S6A). T cells in the central nervous system (CNS) of rats with EAE were initially a mixture of $CD4^+CCR7^+$ naive and Tcm and $CD4^+CCR7^-$ Tem cells because of the adjuvant effect, but as the disease progressed, the majority of T cells in the rat CNS were $CD4^+CCR7^-$ Tem cells (Figure S6B) similar to T cells in the CNS in human MS patients (Kivisakk et al., 2004; Rus et al., 2005). Daily subcutaneous administration of ShK-186 from disease onset had no effect on the initial phase of EAE, but produced a striking reduction in the clinical score, coincident with the emergence of the Tem population in the CNS (Figure 7G). Disease amelioration was accompanied by reduced demyelination and inflammatory infiltrate in the CNS (Figure S6C and Table S1). The presence of inflammatory cells in the CNS of treated rats is consistent with the two-photon DTH data, where Tem cells enter but are immobilized in inflamed tissues in ShK-186-treated rats.

Although Kv1.3 blockers have been previously shown to have a good safety profile in rats and monkeys (Beeton et al., 2006), the primary concern in development of an autoimmune therapy is whether it compromises the protective immune response. We examined whether ShK-186, at the dose that suppresses DTH and chronic EAE, would affect clearance of two medically important infections: influenza and chlamydia. In addition, we examined effects of another Kv1.3-selective blocker, PAP1 (Azam et al., 2007). As a control, we used dexamethasone, which broadly suppresses the immune response. Vehicle-treated Sprague Dawley rats cleared the influenza virus in 4 days, as did rats treated with ShK-186 or PAP-1, whereas dexamethasone significantly delayed clearance (Figure 7H and Figure S7A). In a parallel study, Lewis rats given saline or ShK-186 cleared a chlamydial infection equally rapidly, whereas rats treated with dexamethasone did not clear the infection during the 4 weeks of observation (Figure 7I and Figure S7B).

DISCUSSION

Delayed-type hypersensitivity is an inflammatory immune response initiated by the activation of $CD4^+$ Tem cells, followed by recruitment of macrophages and other effector cells (Szabo et al., 2003). To image the cellular dynamics of this process, we developed a method enabling in situ two-photon microscopy in inflamed ear tissue. We provide the first visualization of Tem cell motility and interaction with APCs and collagen structural elements in peripheral tissue during a DTH immune response. Moreover, we report that a specific blocker of the voltage-gated Kv1.3 potassium channel (ShK-186) inhibits DTH and suppresses Tem effector cell activation in inflamed tissues, but does not alter acute immune clearance in two infectious-disease models.

At the onset of DTH, cytokine cross-talk between tissue-resident APCs and skin-homing T cells initiates an inflammatory cascade. Three hours after antigen challenge, we find that Ova-specific Tem cells are predominantly engaged in prolonged contacts with tissue-resident APCs in the subcutaneous tissue and display low overall motility. In contrast, antigen-irrelevant Tem

cells are highly motile in the inflamed tissue. This mirrors the behavior of myelin basic protein-specific Tem cells invading the spinal cord, where many of the cells appeared tethered to a fixed point (Kawakami et al., 2005). The Ova-specific Tem cells used here were highly motile in spinal cord tissue, but became immobilized after intrathecal injection of Ova, presumably because of interaction with local APCs (Kawakami et al., 2005). Our results extend those observations by showing that during the course of an immune response, Tem effector cells arrest in contact with APCs enlarge and become highly motile through dense networks of collagen. Although less numerous from 24 to 42 hr, the Tem effector cells move rapidly, primarily tracking along bundles with apparently random changes in direction at scaffold junctions, but also occasionally traversing between bundles. Such directionality contrasts with the random motility of these same cells in spinal cord (Kawakami et al., 2005), and with the random motion of $CCR7^+$ cells in lymph node (Miller et al., 2002).

When Tem cells encounter cognate-antigen-bearing APCs in the ear tissue, they enter an activation cascade that is mirrored by changes in cell dynamics. As the cells activate, Ca^{2+} signaling is initiated; motility is arrested; and the cells enlarge, produce cytokines, and alter gene expression in preparation for cell proliferation. The enlarged T cell blasts later release from the APCs and migrate rapidly along collagen fibers, while continuing to have further encounters with APCs. In vitro studies have shown that Ca^{2+} signaling is required for stable T cell-APC association and alterations in gene expression (Negulescu et al., 1996, 1994). If ShK-186 is present, Ca^{2+} signaling is attenuated, resulting in reduced activation of β1 integrin and suppression of cytokine production and cell proliferation (Beeton et al., 2006). Consequently, Tem cells do not reactivate at the site of DTH in rats treated with ShK-186, as indicated by their failure to form productive contacts with APCs or enlarge. The attenuated calcium signaling and reduced activated β1 integrin expression probably contribute to the nonmotile state of the Tem cells. Integrins α1β1 (VLA-1) and α2β1 (VLA-2) enable lymphocytes to adhere to collagen in inflamed tissue (de Fougerolles et al., 2000), and in this study α1β1 and α4β1 (VLA-4) are both upregulated by Ova-specific GFP^+ Tem cells that are found tracking along collagen in ear tissue. Together, our results and those of others (reviewed in Dustin and de Fougerolles [2001]) indicate that normal Ca^{2+} signaling and maintenance of activated b1 integrin in Tem cells are necessary for Tem cell activation and subsequent motility in the collagen-rich tissue environment.

Altered motility and suppression of Ca^{2+} signaling provide a plausible mechanism for the selectivity and effectiveness of Kv1.3 blockers in preventing or treating disease in five distinct autoimmune models that are mediated by Tem cells: EAE in Lewis rats induced by adoptively transferred myelin-specific Tem cells (MS model) (Beeton et al., 2005; Beeton et al., 2001), chronic relapsing-remitting EAE in DA rats (MS model) (Figure 7G), pristane-induced arthritis in DA rats (RA model) (Beeton et al., 2006), experimental autoimmune diabetes mellitus in BB rats (T1DM model) (Beeton et al., 2006), and allergic contact dermatitis (Azam et al., 2007). Kv1.3 channel blockade during treatment of an autoimmune or inflammatory condition would reduce the ability of T cells to locate APCs in the tissue environment and Ca^{2+} signaling and downstream activation responses by T cells that do make contact with APCs. Currently available immunosuppressive agents, including natalizumab (Tysabri), a VLA4 antagonist that prevents effectors from entering tissues (Li et al., 2006), and $S1P_1$-receptor-antagonists (e.g., FTY720) that regulate lymphocyte trafficking at vascular endothelial and lymphatic endothelial barriers (Rosen et al., 2007), are less selective for Tem cells.

The Kv1.3 channel in Tem cells is an important molecular target in inflammatory and autoimmune disorders. Tem cells are implicated in the pathogenesis of MS, and therapies that selectively target Tem cells, while sparing naive and Tcm cells, may have utility in MS therapy (Beeton et al., 2006; Haegele et al., 2007; Hu et al., 2007; Kivisakk et al., 2004; Krakauer et al., 2006; Rus et al., 2005; Wulff et al., 2003a). The normal timeline to clearance of influenza

virus and *Chlamydia trachomatis* in rats treated with a DTH-suppressing dose of ShK-186 is probably the result of redundancy in the multiple types of immune cells and cellular mechanisms involved in the clearance of these infectious agents. Preferential suppression of Tem cells in psoriasis patients by Alefacept (Ellis and Krueger, 2001) does not enhance the frequency of infections, and patients receiving Alefacept mount adequate vaccine antibody responses (Goffe et al., 2005; Gottlieb et al., 2003). In addition, Kv1.3 blockers are not expected to compromise anti-tumor immune responses (Klebanoff et al., 2005), or responses to chronic infections (Heydtmann et al., 2006; Stubbe et al., 2006), which are more effectively mediated by Tcm cells than by Tem cells.

In summary, our two-photon imaging methodology reveals the Tem cell dynamics underlying the normal immune response in peripheral tissues and provides mechanistic insights into the therapeutic potential of immunosuppression by targeting the Kv1.3 channels on Tem cells. The profound effects of Kv1.3 blockers on the motility and activation of Tem cells at the tissue site of antigen challenge suggest a promising strategy for treatment of chronic autoimmune diseases mediated by autoreactive Tem cells, a therapy based upon prolonged immobilization of Tem effectors at sites of inflammation and by preventing effectors from making contact with APCs and receiving activation signals.

EXPERIMENTAL PROCEDURES

Animals

Female inbred Lewis and DA rats were purchased from Harlan-Sprague Dawley (Indianapolis, IN, USA), and female inbred Sprague Dawley rats were purchased from Charles River (Raleigh, NC, USA). Animals were housed under clean conditions with irradiated rodent chow and acidified water ad libitum. All procedures were in accordance with National Institutes of Health (NIH) guidelines and approved by the University of California, Irvine, Institutional Animal Care and Use Committee.

Cells

Lewis ratOva-specificCD4$^+$Tcells transducedwithGFP(Flugel et al., 1999)were maintained in culture by alternating phases of expansion in medium containing T cell growth factor (TCGF) and phases of stimulation with Ova (Sigma, St. Louis, MO, USA) in the presence of irradiated thymocytes as antigen-presenting cells, as described (Beeton et al., 2001). See Supplemental Experimental Procedures for additional details. T cells were isolated from Lewis rat spleens and lymph nodes with a MACS separation column (Miltenyi Biotec, Auburn, CA, USA). Purities of CD3$^+$ and of CD4$^+$ T cells were >95%, as indicated by flow cytometry.

Potassium-Channel Blockers

ShK-186 was synthesized as described (Beeton et al., 2005). PAP-1 (Schmitz et al., 2005) was a kind gift from H. Wulff (UC Davis, CA).

Delayed-Type Hypersensitivity and Administration of ShK-186

Adoptive DTH was induced in 7- to 9-week-old Lewis rats by the intraperitoneal transfer of 10×10^6 GFP$^+$ Ova-activated effector T cells (Beeton and Chandy, 2007). Rats were challenged 48 hr later with 20 μg Ova-TR in the pinna of the right ear and saline in the pinna of the left ear. Rats received subcutaneous injections in the scruff of the neck of ShK-186 (100 μg/kg/day) or vehicle (PBS + 2% Lewis rat serum) at the time of challenge and 24 hr later. Induction of active DTH with the nonrelevant antigen HEL was initiated by priming 7- to 9-week-old Lewis rats with an intradermal injection of emulsion of HEL (100 μg/rat) in complete Freund's adjuvant (Difco, Detroit, MI, USA). Five days later, 10 million activated Ova-GFP T cells were

injected intraperitoneally. Two days later, the rats were challenged with an injection of HEL dissolved in saline in the pinna of one ear (20 μg/20 μl) and saline in the other ear. Ear thickness was measured at the site of injection 3, 24, and 42 hr after challenge with a spring-loaded micrometer (Mitutoyo, Spokane, WA, USA) and the difference in ear Ova-TR versus saline-challenged ears was calculated. Statistical analysis was carried out with the Mann-Whitney U test.

Tissue Preparation

DTH in rat ears is characterized by effector T cell infiltration of the subcutaneous tissue and dermis (Hancock et al., 1994). After determining that autofluorescence and second-harmonic signals from hair follicles obscured visualization of inflammatory cells and antigen-bearing APCs, we developed a method to expose the subcutaneous tissue of the ear for imaging during DTH. Lewis rats with DTH were euthanized 3, 24, or 42 hr after challenge, and after cardiac perfusion, the ears were removed by a single angled slice and kept in $C0_2$-independent media on ice. Under a 10× dissecting micro-scope, edges of the ear (~2 mm of tissue on each side) were removed to aid in separation of the epidermis and dermis together with the hair follicles. Tissue separation began at the proximal end of the ear with iridectomy dissection scissors (3 mm Vannas style, Fine Science Tools, Foster City, CA, USA) used to cut small extensions of connective tissue between the two layers. The preparation was then immediately mounted under the two-photon microscope, with the exposed subcutaneous tissue on the dorsal side of the ear facing the objective lens. Subsequent hemotoxylin and eosin staining of sections from imaged tissue confirmed tissue integrity.

Footpad DTH and Intravital Imaging

Adoptive DTH in the footpad of 7- to 9-week-old Lewis rats was induced by the intraperitoneal transfer of 10×10^6 GFP^+ Ova-activated effector T cells (Beeton and Chandy, 2007), followed by antigen challenge 48 hr later with 20 mg Ova-TR in the right front paw. Twenty-four hours after antigen challenge, animals were anesthetized with 100 mg/kg ketamine, 10 mg/kg xylene, and 1/2 dosages were given every 45 min after initial anesthesia dose. The imaged paw was immobilized in a liquid-tight chamber filled with prewarmed RPMI for two-photon imaging of the ventral surface. DTH reaction was assessed by paw swelling and visualization of inflamed tissue marked by redness and observation of animal preference for the alternate forepaw.

Two-Photon Imaging and Data Analysis

Two-photon imaging was performed as described previously (Matheu et al., 2007; Miller et al., 2002), with an upright Olympus BX50 microscope fitted with a 20× water-immersion objective (numerical aperture 0.95), a Spectra-Physics Tsunami femto-second laser, a resonant-mirror scan head, and a motorized focus controller (Prior Scientific, Rockland, MA, USA) (Nguyen et al., 2001). Images were acquired under software control by METAMORPH (Universal Imaging, Downingtown, PA, USA). Three-dimensional (3D) image stacks in ear tissue (x, y, z) were acquired at 18 s time intervals through an imaging volume 50 mm deep. Images and movies were processed with the 3D analysis software IMARIS 5.5.3., 64-bit version (Bitplane AG, Saint Paul, MN, USA). Three-dimensional graphs were prepared with ED Grapher (RomanLab Software, Vancouver, British Columbia, Canada). An excitation wavelength of 890 gave optimal second-harmonic generation from collagen together with two-photon excitation of GFT and TR, and these signals were imaged with three photomultiplier channels (respectively, blue, green, and red) in conjunction with 500 nm and 560 nm dichroic mirrors and a 510 nm long-pass filter. Cell size was measured as cross-sectional (x-y) area, with an ellipsoid shape approximation. Data are presented as mean ± 1 standard error of the mean (SEM). Tests of statistical significance were performed with a two-tailed Student's t test,

or Mann-Whitney U test where indicated. Significance is denoted in figures as * = 0.05; ** = 0.01; *** = 0.001; **** = 0.0001.

T Cell Motility in the Lymph Node

$CD3^+$ T cells were purified from Lewis rat spleen and lymph nodes (Miltenyi Biotech cell-separation kit: 130-090–320), labeled with 4 mm carboxyfluores-cein diacetate succinimidyl ester (CFSE, Invitrogen) for 30 min and adoptively transferred by tail-vein injection. Concurrent with adoptive transfer, animals received a subcutaneous injection of either saline or ShK-186 (100 μg/kg). Animals were euthanized 3 hr after adoptive transfer and treatment. Inguinal, axillary, and cervical lymph nodes were removed and imaged as previously described (Miller et al., 2002). T cell recovery from lymph node was determined as percent recovered, normalized by total weight of lymph node tissue.

Homing of Ova T Cells to the Ears

For measurement of homing of the Ova-specific $CCR7^-$ effector T cells to the ears of Lewis rats with DTH, animals were euthanized 3, 24, or 42 hr after challenge. Ears were removed after cardiac perfusion with saline. Single-cell suspensions were prepared and analyzed for the presence of GFP^+ cells on a BD FACSCalibur with CellQuest software (BD Biosciences, San Jose, CA, USA).

Electrophysiology

Ova-T cells were patch-clamped in the whole-cell configuration at rest and 48 hr after activation with Ova as described (Wulff et al., 2003b). See Supplemental Experimental Procedures for additional details.

Calcium Imaging

Ratiometric calcium imaging was performed with Tem cells loaded with Fura-2 as described (Fanger et al., 2001), with cell-based calibration using ionomycin and EGTA or 10 mM external Ca^{2+} to achieve R_{min} and R_{max}, respectively.

In Vitro Assessment of Activated β1 Integrin

In the adoptive DTH model, Ova-specific Tem cells were activated in vitro for 48 hr before adoptive transfer into rats. Therefore, for the HUTS staining experiment, we activated the cells in vitro for 48 hr before assessing the effect of ShK-186 on HUTS expression. Cells were stained with monocolonal HUTS-21 (BD Biosciences), which recognizes an epitope among amino acids 355– 425 that is exposed upon activation of b1 integrin (Luque et al., 1996). FACS analysis of HUTS-21 staining was performed by gating on the GFP^+ cell population. The observed shift in mean fluorescence ratio of activated cells is consistent with previous studies (Gomez et al., 1997; Levite et al., 2000; Luque et al., 1996). See Supplemental Experimental Procedures for additional details.

Proliferation Assays

Effect of ShK-186 on the proliferation of Ova GFP^+ Tem cells was determined with [^{3}H]-thymidine incorporation assays as described (Beeton et al., 2005; Beeton et al., 2001). See Supplemental Experimental Procedures for additional details.

Supplementary Material

Refer to Web version on PubMed Central for supplementary material.

ACKNOWLEDGMENTS

We wish to thank R. Paquette for assistance with reagent preparation and D. Sen for advice on movie compression. We also thank B. Andersen and S. Griffey for helpful discussions and advice. M.P.M. was supported by a NIH Ruth L. Kirchstein predoctoral fellowship AI-64128. A.G. was supported by a NIH Minority Supplement. M.U. was supported by a 2006–2007 Medical Student Research Grant from the American Heart Association Western States Affiliates. AIRMID Inc. supported the good laboratory practices (GLP) studies at the Burleson Research Technologies to examine the effect of Kv1.3 blockers on rat-adapted influenza virus in rats. Additional support was provided by the Hertie Foundation (#1.01.1/04/010) and the Deutsche Forschungsgemeinschaft (SFB455) (A.F.); the American Heart Association Western States Affiliates (0665009Y) (C.B.); and NIH grants GM-41514 (M.D.C.), NS-48252 (K.G.C.), GM-48071 (I.P.), and AI-32248 (L.M.d.l.M.).

REFERENCES

Andreasen SO, Thomsen AR, Koteliansky VE, Novobrantseva TI, Sprague AG, de Fougerolles AR, Christensen JP. Expression and functional importance of collagen-binding integrins, alpha 1 beta 1 and alpha 2 beta 1, on virus-activated T cells. J. Immunol 2003;171:2804–2811. [PubMed: 12960301]

Azam P, Sankaranarayanan A, Homerick D, Griffey S, Wulff H. Targeting effector memory T cells with the small molecule Kv1.3 blocker PAP-1 suppresses allergic contact dermatitis. J. Invest. Dermatol 2007;127:1419–1429. [PubMed: 17273162]

Beeton C, Chandy KG. Induction and monitoring of adoptive delayed type hypersensitivity in rats. J. Visualized Experiments 8. 2007Published online October 1 2007. 10.3791/325

Beeton C, Wulff H, Barbaria J, Clot-Faybesse O, Pennington M, Bernard D, Cahalan MD, Chandy KG, Beraud E. Selective blockade of T lymphocyte K+ channels ameliorates experimental autoimmune encephalomyelitis, a model for multiple sclerosis. Proc. Natl. Acad. Sci. USA 2001:13942–13947. [PubMed: 11717451]

Beeton C, Pennington MW, Wulff H, Singh S, Nugent D, Crossley G, Khaytin I, Calabresi PA, Chen CY, Gutman GA, Chandy KG. Targeting effector memory T cells with a selective peptide inhibitor of Kv1.3 channels for therapy of autoimmune diseases. Mol. Pharmacol 2005;67:1369–1381. [PubMed: 15665253]

Beeton C, Wulff H, Standifer NE, Azam P, Mullen KM, Pennington MW, Kolski-Andreaco A, Wei E, Grino A, Counts DR, et al. Kv1.3 channels are a therapeutic target for T cell-mediated autoimmune diseases. Proc. Natl. Acad. Sci. USA 2006;103:17414–17419. [PubMed: 17088564]

Chandy KG, Wulff H, Beeton C, Pennington M, Gutman GA, Cahalan MD. K^+ channels as targets for specific immunomodulation. Trends Pharmacol. Sci 2004;25:280–289. [PubMed: 15120495]

Conrad C, Boyman O, Tonel G, Tun-Kyi A, Laggner U, de Fougerolles A, Kotelianski V, Gardner H, Nestle FO. alpha(1)beta(1) integrin is crucial for accumulation of epidermal T cells and the development of psoriasis. Nat. Med 2007;13:836–842. [PubMed: 17603494]

de Fougerolles AR, Sprague AG, Nickerson-Nutter CL, Chi-Rosso G, Rennert PD, Gardner H, Gotwals PJ, Lobb RR, Koteliansky VE. Regulation of inflammation by collagen-binding integrins alpha1beta1 and alpha2beta1 in models of hypersensitivity and arthritis. J. Clin. Invest 2000;105:721–729. [PubMed: 10727440]

Dustin ML, de Fougerolles AR. Reprogramming T cells: The role of extracellular matrix in coordination of T cell activation and migration. Curr. Opin. Immunol 2001;13:286–290. [PubMed: 11406359]

Ellis CN, Krueger GG. Treatment of chronic plaque psoriasis by selective targeting of memory effector T lymphocytes. N. Engl. J. Med 2001;345:248–255. [PubMed: 11474662]

Fanger CM, Rauer H, Neben AL, Miller MJ, Wulff H, Rosa JC, Ganel-lin CR, Chandy KG, Cahalan MD. Calcium-activated potassium channels sustain calcium signaling in T lymphocytes. Selective blockers and manipulated channel expression levels. J. Biol. Chem 2001;276:12249–12256. [PubMed: 11278890]

Ferguson TA, Mizutani H, Kupper TS. Two integrin-binding peptides abrogate T cell-mediated immune responses in vivo. Proc. Natl. Acad. Sci. USA 1991;88:8072–8076. [PubMed: 1896454]

Flugel A, Willem M, Berkowicz T, Wekerle H. Gene transfer into $CD4^+$ T lymphocytes: Green fluorescent protein-engineered, encephalitogenic T cells illuminate brain autoimmune responses. Nat. Med 1999;5:843–847. [PubMed: 10395334]

Gaga M, Frew AJ, Varney VA, Kay AB. Eosinophil activation and T lymphocyte infiltration in allergen-induced late phase skin reactions and classical delayed-type hypersensitivity. J. Immunol 1991;147:816–822. [PubMed: 1830598]

Goffe B, Papp K, Gratton D, Krueger GG, Darif M, Lee S, Bozic C, Sweetser MT, Ticho B. An integrated analysis of thirteen trials summarizing the long-term safety of alefacept in psoriasis patients who have received up to nine courses of therapy. Clin. Ther 2005;27:1912–1921. [PubMed: 16507377]

Gomez M, Luque A, delPozo MA, Hogg N, Sanchez-Madrid F, Cabanas C. Functional relevance during lymphocyte migration and cellular localization of activated beta1 integrins. Eur. J. Immunol 1997;27:8–16. [PubMed: 9021992]

Gottlieb AB, Casale TB, Frankel E, Goffe B, Lowe N, Ochs HD, Roberts JL, Washenik K, Vaishnaw AK, Gordon KB. $CD4^+$ T-cell-directed antibody responses are maintained in patients with psoriasis receiving alefacept: Results of a randomized study. J. Am. Acad. Dermatol 2003;49:816–825. [PubMed: 14576659]

Haegele KF, Stueckle CA, Malin JP, Sindern E. Increase of $CD8^+$ T-effector memory cells in peripheral blood of patients with relapsing-remitting multiple sclerosis compared to healthy controls. J. Neuroimmunol 2007;183:168–174. [PubMed: 17084910]

Hancock WW, Khoury SJ, Carpenter CB, Sayegh MH. Differential effects of oral versus intrathymic administration of polymorphic major histocompatibility complex class II peptides on mononuclear and endothelial cell activation and cytokine expression during a delayed-type hypersensitivity response. Am. J. Pathol 1994;144:1149–1158. [PubMed: 8203456]

Heydtmann M, Hardie D, Shields PL, Faint J, Buckley CD, Campbell JJ, Salmon M, Adams DH. Detailed analysis of intrahepatic CD8 T cells in the normal and hepatitis C-infected liver reveals differences in specific populations of memory cells with distinct homing phenotypes. J. Immunol 2006;177:729–738. [PubMed: 16785572]

Hu L, Pennington M, Jiang Q, Whartenby KA, Calabresi PA. Characterization of the functional properties of the voltage-gated potassium channel Kv1.3 in human $CD4^+$ T lymphocytes. J. Immunol 2007;179:4563–4570. [PubMed: 17878353]

Kawakami N, Nagerl UV, Odoardi F, Bonhoeffer T, Wekerle H, Flugel A. Live imaging of effector cell trafficking and autoantigen recognition within the unfolding autoimmune encephalomyelitis lesion. J. Exp. Med 2005;201:1805–1814. [PubMed: 15939794]

Kivisakk P, Mahad DJ, Callahan MK, Sikora K, Trebst C, Tucky B, Wujek J, Ravid R, Staugaitis SM, Lassmann H, Ransohoff RM. Expression of CCR7 in multiple sclerosis: Implications for CNS immunity. Ann. Neurol 2004;55:627–638. [PubMed: 15122702]

Klebanoff CA, Gattinoni L, Torabi-Parizi P, Kerstann K, Cardones AR, Finkelstein SE, Palmer DC, Antony PA, Hwang ST, Rosenberg SA, et al. Central memory self/tumor-reactive $CD8^+$ T cells confer superior antitumor immunity compared with effector memory T cells. Proc. Natl. Acad. Sci. USA 2005;102:9571–9576. [PubMed: 15980149]

Krakauer M, Sorensen PS, Sellebjerg F. $CD4^+$ memory T cells with high CD26 surface expression are enriched for Th1 markers and correlate with clinical severity of multiple sclerosis. J. Neuroimmunol 2006;181:157–164. [PubMed: 17081623]

Levite M, Cahalon L, Peretz A, Hershkoviz R, Sobko A, Ariel A, Desai R, Attali B, Lider O. Extracellular K^+ and opening of voltage-gated potassium channels activate T cell integrin function: Physical and functional association between Kv1.3 channels and beta1 integrins. J. Exp. Med 2000;191:1167–1176. [PubMed: 10748234]

Li YY, Perez HD, Zollner TM. Fatalities in natalizumab treatment-a ‘no go’ for leukocyte recirculation approaches? Expert Opin. Ther. Targets 2006;10:489–499.

Lim YC, Wakelin MW, Henault L, Goetz DJ, Yednock T, Cabanas C, Sanchez-Madrid F, Lichtman AH, Luscinskas FW. Alpha4-beta1-integrin activation is necessary for high-efficiency T-cell subset interactions with VCAM-1 under flow. Microcirculation 2000;7:201–214. [PubMed: 10901499]

Luque A, Gomez M, Puzon W, Takada Y, Sanchez-Madrid F, Cabanas C. Activated conformations of very late activation integrins detected by a group of antibodies (HUTS) specific for a novel regulatory region (355–425) of the common beta 1 chain. J. Biol. Chem 1996;271:11067–11075. [PubMed: 8626649]

Mackay CR, Marston WL, Dudler L, Spertini O, Tedder TF, Hein WR. Tissue-specific migration pathways by phenotypically distinct subpopulations of memory T cells. Eur. J. Immunol 1992;22:887–895. [PubMed: 1372559]

Matheu MP, Deane JA, Parker I, Fruman DA, Cahalan MD. Class IA phosphoinositide 3-kinase modulates basal lymphocyte motility in the lymph node. J. Immunol 2007;179:2261–2269. [PubMed: 17675487]

Miller MJ, Wei SH, Parker I, Cahalan MD. Two-photon imaging of lymphocyte motility and antigen response in intact lymph node. Science 2002;296:1869–1873. [PubMed: 12016203]

Negulescu PA, Shastri N, Cahalan MD. Intracellular calcium dependence of gene expression in single T lymphocytes. Proc. Natl. Acad. Sci. USA 1994;91:2873–2877. [PubMed: 8146203]

Negulescu PA, Krasieva TB, Khan A, Kerschbaum HH, Cahalan MD. Polarity of T cell shape, motility, and sensitivity to antigen. Immunity 1996;4:421–430. [PubMed: 8630728]

Nguyen QT, Callamaras N, Hsieh C, Parker I. Construction of a two-photon microscope for video-rate Ca^{2+} imaging. Cell Calcium 2001;30:383–393. [PubMed: 11728133]

Panyi G, Vamosi G, Bacso Z, Bagdany M, Bodnar A, Varga Z, Gaspar R, Matyus L, Damjanovich S. Kv1.3 potassium channels are localized in the immunological synapse formed between cytotoxic and target cells. Proc. Natl. Acad. Sci. USA 2004;101:1285–1290. [PubMed: 14745040]

Pereira LE, Villinger F, Wulff H, Sankaranarayanan A, Raman G, An-sari AA. Pharmacokinetics, toxicity, and functional studies of the selective kv1.3 channel blocker 5-(4-phenoxybutoxy)psoralen in rhesus macaques. Exp. Biol. Med. (Maywood) 2007;232:1338–1354. [PubMed: 17959847]

Picker LJ, Terstappen LW, Rott LS, Streeter PR, Stein H, Butcher EC. Differential expression of homing-associated adhesion molecules by T cell subsets in man. J. Immunol 1990;145:3247–3255. [PubMed: 1700003]

Rosen H, Sanna MG, Cahalan SM, Gonzalez-Cabrera PJ. Tipping the gatekeeper: S1P regulation of endothelial barrier function. Trends Immunol 2007;28:102–107. [PubMed: 17276731]

Rowin ME, Whatley RE, Yednock T, Bohnsack JF. Intracellular calcium requirements for beta1 integrin activation. J. Cell. Physiol 1998;175:193–202. [PubMed: 9525478]

Rus H, Pardo CA, Hu L, Darrah E, Cudrici C, Niculescu T, Niculescu F, Mullen KM, Allie R, Guo L, et al. The voltage-gated potassium channel Kv1.3 is highly expressed on inflammatory infiltrates in multiple sclerosis brain. Proc. Natl. Acad. Sci. USA 2005;102:11094–11099. [PubMed: 16043714]

Sallusto F, Geginat J, Lanzavecchia A. Central memory and effector memory T cell subsets: Function, generation, and maintenance. Annu. Rev. Immunol 2004;22:745–763. [PubMed: 15032595]

Schmitz A, Sankaranarayanan A, Azam P, Schmidt-Lassen K, Homerick D, Hansel W, Wulff H. Design of PAP-1, a selective small molecule Kv1.3 blocker, for the suppression of effector memory T cells in autoimmune diseases. Mol. Pharmacol 2005;68:1254–1270. [PubMed: 16099841]

Soler D, Humphreys TL, Spinola SM, Campbell JJ. CCR4 versus CCR10 in human cutaneous TH lymphocyte trafficking. Blood 2003;101:1677–1682. [PubMed: 12406880]

Stubbe M, Vanderheyde N, Goldman M, Marchant A. Antigen-specific central memory $CD4^+$ T lymphocytes produce multiple cytokines and proliferate in vivo in humans. J. Immunol 2006;177:8185–8190. [PubMed: 17114495]

Szabo SJ, Sullivan BM, Peng SL, Glimcher LH. Molecular mechanisms regulating Th1 immune responses. Annu. Rev. Immunol 2003;21:713–758. [PubMed: 12500979]

Wulff H, Beeton C, Chandy KG. Potassium channels as therapeutic targets for autoimmune disorders. Curr. Opin. Drug Discov. Devel 2003a;6:640–647.

Wulff H, Calabresi PA, Allie R, Yun S, Pennington M, Beeton C, Chandy KG. The voltage-gated Kv1.3 K^+ channel in effector memory T cells as new target for MS. J. Clin. Invest 2003b;111:1703–1713. [PubMed: 12782673]

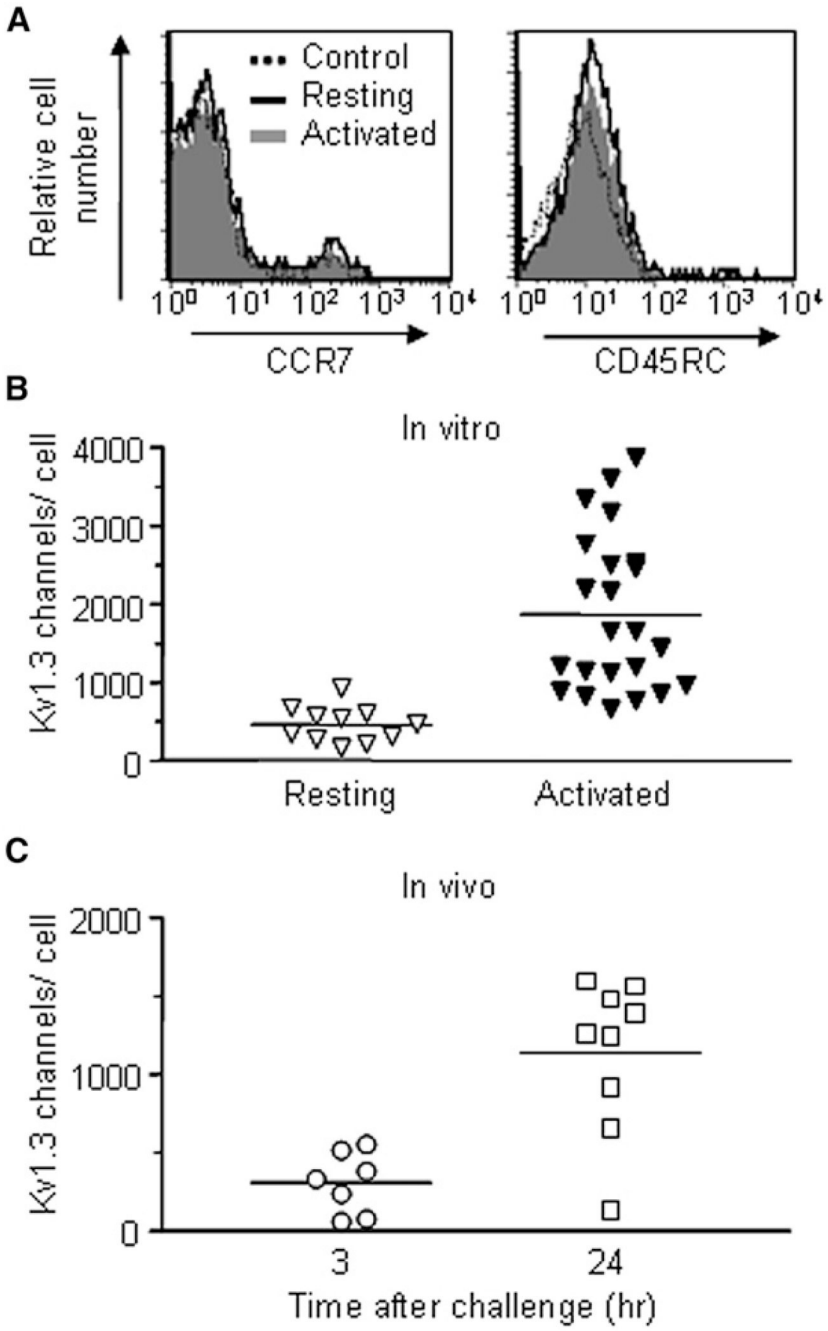

Figure 1. Characterization of Ova-GFP T Cells

(A) Flow-cytometric analysis of the indicated cell-surface proteins on Ova-specific GFP^+ $CD4^+$ rat T cells. The cells are $CCR7^-$ $CD45RC^-$, characteristic of Tem cells (solid line = resting Ova-GFP^+ T cells, dotted line = background staining; gray = activated).

(B) Kv1.3 channel expression in resting (mean = 461 ± 69 Kv1.3 channels/cell, n = 11 cells) and activated (1862 ± 208 Kv1.3 channels/cell, n = 23)GFP^+ $CD4^+$ Ova-specific rat T cells. Data were obtained by patch-clamp analysis.

(C) Kv1.3 channel expression in GFP^+ Ova-specific T cells isolated from ears undergoing DTH, 3 hr (307 ± 74 Kv1.3 channels/cell, n = 7 cells) and 24 hr (1136 ± 162 Kv1.3 channels/cell, n = 9 cells) after challenge with Ova.

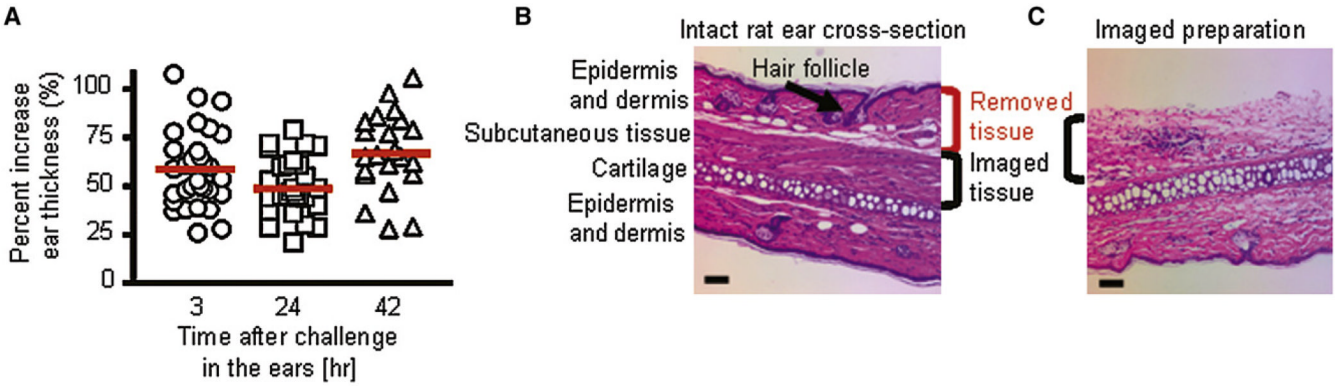

Figure 2. Induction of Adoptive DTH

(A) DTH assessed by measurement ofthe difference inear thickness(Δ ear thickness) between the Ova-TR-injected ear and the saline-injected ear and plotted as % change at different times after antigen challenge.

(B) Hematoxylin and Eosin stain of a cross-section through an intact rat ear showing the various tissue layers, and indicating those layers removed for imaging. The scale bar represents 50 μm.

(C) Rat ear section from an imaged preparation stained with Hematoxylin and Eosin. The scale bar represents 50 μm.

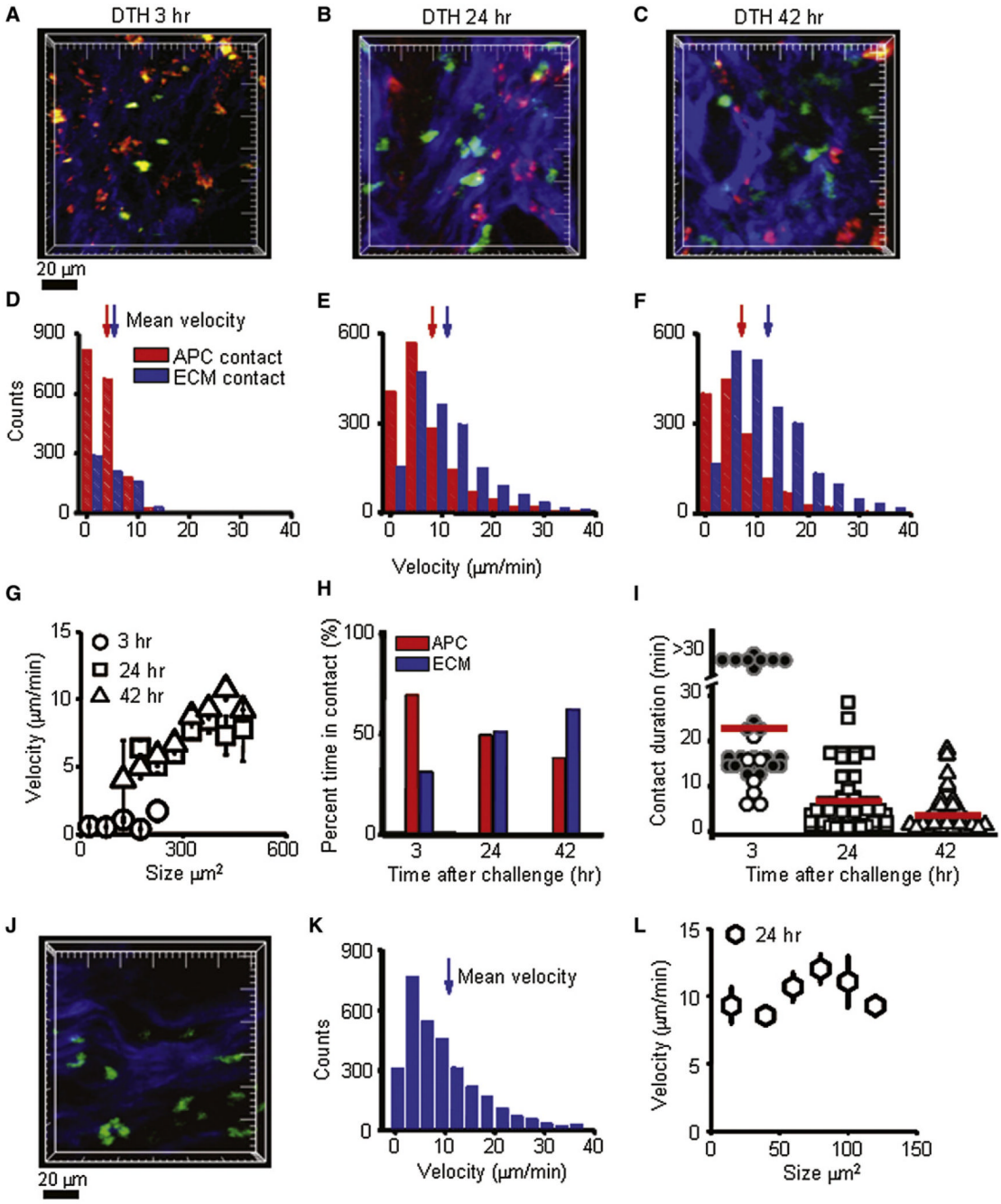

Figure 3. Activation and Motility of CCR7 Effector Cells at the Site of DTH

(A) GFP$^+$ Ova-specific T cells (green) in subcutaneous ear tissue 3 hr after antigen injection interacting with local APCs (red) among collagen fibers (blue). Major tick marks = 20 µm.

(B) Enlarged, highly motile CCR7$^-$ effector cells (green) 24 hr after antigen injection, imaged crawling along collagen-fiber bundles.

(C) Large, highly motile CCR7$^-$ effectors in the subcutaneous tissue 42 hr after antigen injection.

(D) Distributions of instantaneous velocities of CCR7$^-$ effector cells at 3 hr. Those in contact with an APC are shown by red bars (mean velocity 3.9 µm/min, n = 1722 measurements); those in contact with collagen are shown by blue bars (5.3 µm/min, n = 758; $p < 0.05$).

(E) Corresponding velocity distributions of CCR7^{-} effector cells 24 hr after antigen challenge. CCR7^{-} effectors in contact with collagen fibers were highly motile (blue bars, 11.1 μm/min, n = 1654), whereas those contacting antigen-bearing APCs showed lower velocities (red bars, 7.4 μm/min, n = 1568; $p < 0.05$).
(F) Velocity distributions of CCR7^{-} effector cells contacting collagen (blue bars, 12.0 μm/min, n = 2213) or encountering an antigen-bearing APCs (red bars, 7.0 μm/min, n = 1359; $p < 0.05$) measured 42 hr after antigen challenge.
(G) Mean velocities of CCR7^{-} effector cells as a function of their cross-sectional areas at different times during DTH. Values were expressed as mean ± standard error (SE).
(H) Percentages of time for which CCR7^{-} effectors were in contact with local APCs or collagen fibers at 3 hr (APC: 69%, collagen: 31%), 24 hr (APC: 49%, collagen: 51%), and 42 hr (APC: 38%, collagen: 62%) after antigen challenge. $n \geq 50$ cells.
(I) Duration of CCR7^{-} effector T cell contacts with local APCs at varying times after antigen challenge; mean contact durations are represented by red bars at 3 hr (24 min, n = 54 contacts in 6 experiments), 24 hr (7 min, n = 77 contacts in 3 experiments), and 42 hr (3.5 min, n = 55 contacts in 3 experiments).
(J) Bystander GFP^{+} Ova-specific T cells (green) among collagen fibers (blue) in subcutaneous ear tissue 24 hr after induction of active DTH by injection of hen-egg lysozyme (HEL). Development of the DTH response was measured by ear swelling (44% increase in ear thickness, n = 2). Major tick marks = 20 μm.
(K) Velocity distribution of bystander GFP^{+} Ova-specific T cells (mean velocity 10.4 μm/min, n = 5222).
(L) Mean velocities of bystander GFP^{+} Ova-specific T cells as a function of their cross-sectional area 24 hr after induction of active DTH. Values were expressed as mean ± SE.

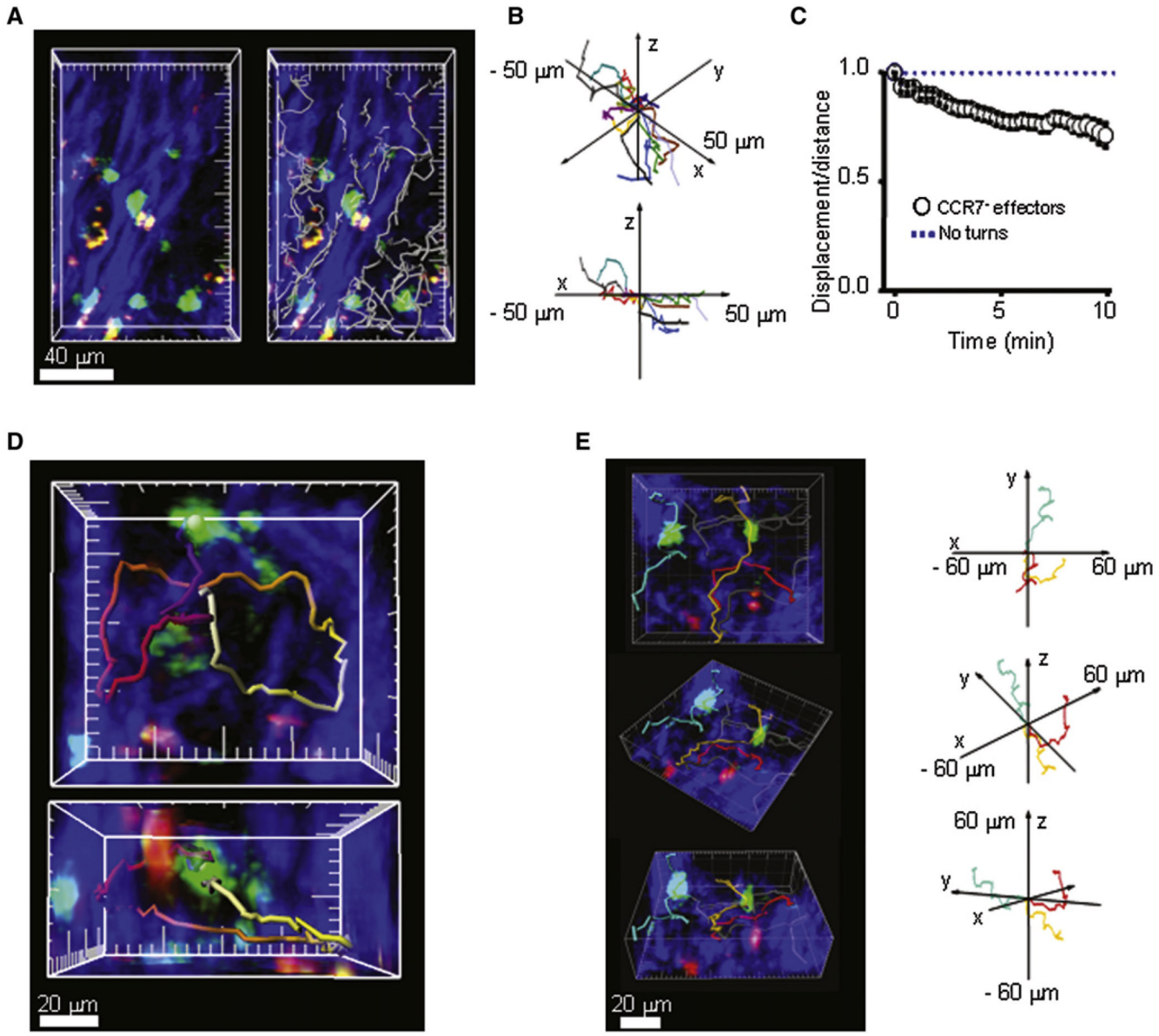

Figure 4. CCR7 Effector Cells Preferentially Crawl along Collagen Fibers

(A) Representative image of effector T cells in the collagen-rich subcutaneous tissue obtained 24 hr after antigen challenge. Left panel is a ‘‘top-view’’ compression through an image stack captured at a single time point; right panel overlays cell tracks recorded throughout a 4 min imaging sequence, illustrating movement of T cells along collagen fibers.

(B) Cell tracks plotted normalizing the orientation of adjacent collagen fibers along the x axis. The 3D plots of effector cell tracks demonstrate preferential motility along the x axis (i.e., parallel to the collagen-fiber bundles).

(C) Meander index (displacement from origin/distance traveled) for effector cells in regions of long collagen fibers (0.75 after 10 min; n = 20 cells). By comparison, the meander index over this period is typically 0.4 for random movement of naive T cells in a lymph node (cf. Figure 7F), and would be 1.0 for cells traveling in a straight line. Values were expressed as mean ± SE.

(D) Cell tracks illustrating the circuitous paths at collagen-fiber junctions. Panels show compressions along the z (upper) and y (lower) axes: tracks are pseudocolored, representing time throughout a 36 min imaging record (purple = start; white = finish). Major tick marks are at 20 μm.

(E) Left panel shows examples of cells moving between adjacent collagen fibers (red and gold tracks) and a cell traversing local collagen structures (turquoise track), depicted in various orientations. Right panel shows 3D plots of these same tracks after normalization of their starting points, and with the turquoise track reoriented to the opposite axis for better visualization.

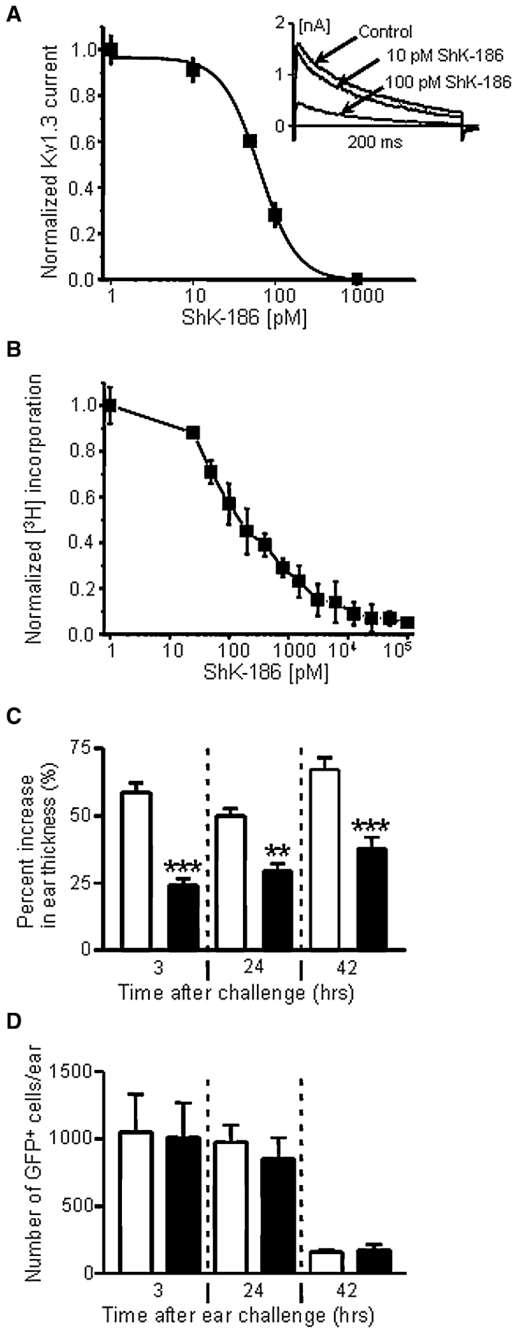

Figure 5. Inhibition of Kv1.3 Currents, Cell Proliferation, and DTH by ShK-186

(A) Dose-dependent inhibition of Kv1.3 currents in Ova-specific GFP^+ $CCR7^-$ effectors by ShK-186. K_d = 65 ± 5 pM; n = 3 cells. Inset shows representative Kv1.3 current traces in the absence or presence of 10 pM or 100 pM ShK-186.

(B) Dose-dependent inhibition of $CCR7^-$ T cell proliferation by ShK-186. IC_{50} = 180 ± 37 pM; n = 3 experiments.

(C) Suppression of DTH-induced ear swelling by administration of 100 μg/kg ShK-186 at the time of antigen challenge and 24 hr after antigen challenge (filled bars), relative to saline-treated rats (open bars). ** $p < 0.01$; *** $p < 0.05$.

(D) Recovery of Ova-specific GFP^+ $CCR7^-$ effectors from whole ear tissue from saline-treated (open bars) and ShK-186-treated animals (filled bars). Rats were extensively cardiac perfused with saline to remove cells from blood vessels before the ears were explanted and analyzed for GFP^+ cells (n = 5 rats). Values were expressed as mean ± standard deviation (SD).

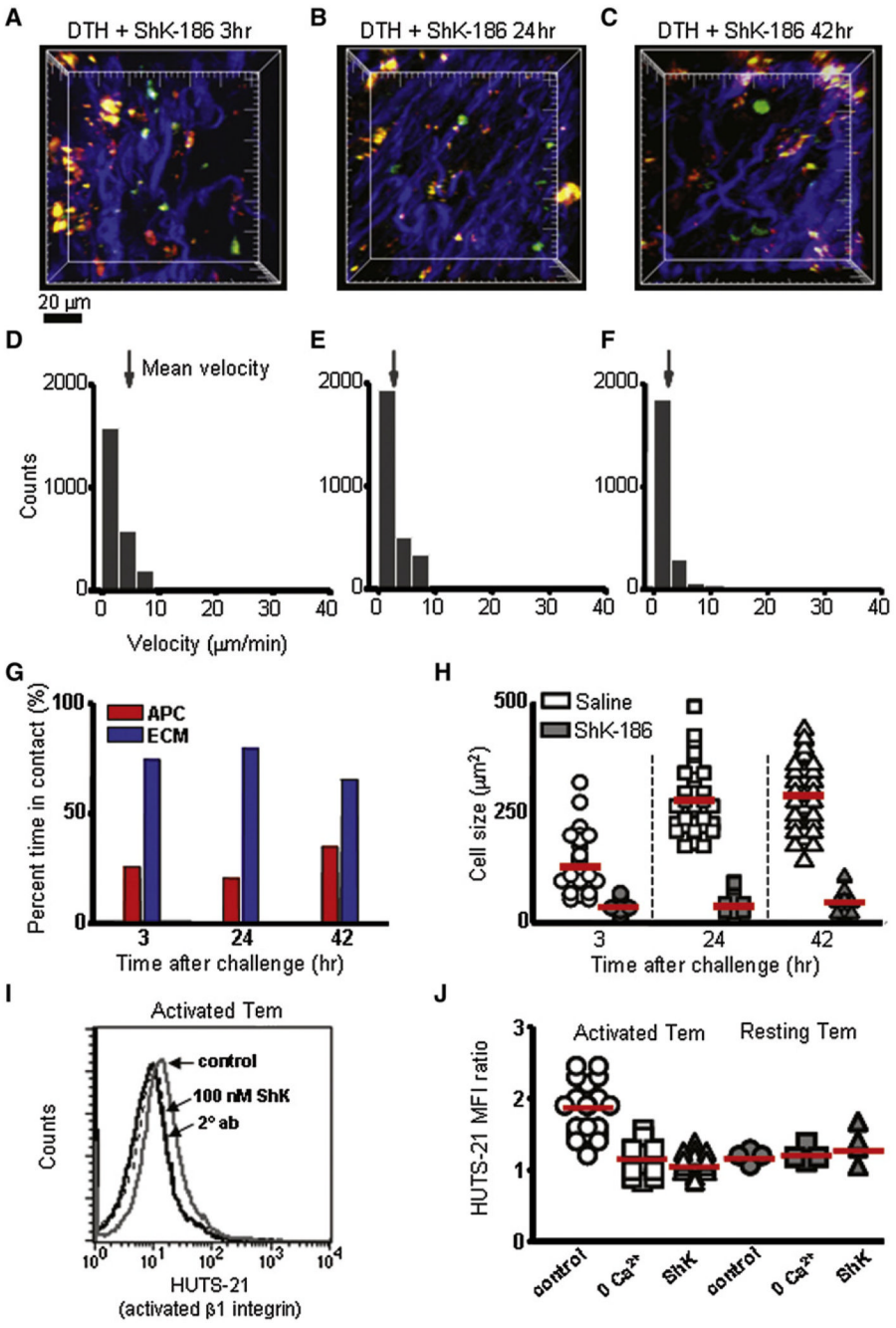

Figure 6. Inhibition of CCR7⁻ Effector Cell Motility and Activation by ShK-186

(A–C) Maximum-intensity projections of two-photon image stacks acquired in the subcutaneous ear tissue at 3, 24, and 42 hr after antigen challenge and treatment with ShK-186. Ova-specific GFP^+ $CCR7^-$ effector cells (green), collagen-fiber bundles (blue), and APCs bearing Ova-TR (red) are shown. Major tick marks = 20 μm.

(D–F) Distributions of instantaneous velocities of $CCR7^-$ effectors cells in ShK-186-treated animals at corresponding time points after Ova-TR challenge. Arrows mark mean velocities (3 hr: 2.7 ± 0.04 μm/min, n = 2397 measurements; 24 hr: 2.1 ± 0.05 μm/min, n = 2870; 42 hr: 1.2 ± 0.04 μm/ min, n = 2227).

(G) Percentage of time effector cells contacted APCs (red bars) or collagen (blue bars) at different time points after Ova-TR challenge (n = 34–46 cells in 3 or 4 experiments).
(H) Sizes (cross-sectional area) of $CCR7^{-}$ effector cells in saline-treated (open symbols) and in ShK-186-treated animals (filled symbols) at different times after Ova-TR challenge. Mean values are indicated by red bars (in saline-treated animals at 3, 24, and 42 hr after antigen challenge, respectively, 130 ± 9.6, 280 ± 11.0 μm^2, and 289 ±11.6 μm^2; in ShK-186-treated animals, 32 ± 2.5, 38 ± 4.1, and 44 ± 4.μm^2).
(I) FACS plots of activated β1 integrin (exposed amino acids 355–425) on the surface of activated Tem cells with and without ShK treatment. Activated Tem cells have the activated form of β1 integrin on the cell surface (gray solid line), which is suppressed by 100 nM ShK-186 (black solid line) to levels similar to control staining (two overlapping dotted lines, left panel).
(J) Mean fluorescence intensity (MFI) ratios (HUTS-21 staining/secondary control) for activated Tem cells (1.8 ± 0.08 SE, n = 21) were significantly higher ($p < 0.01$) than in activated Tem incubated in 0 Ca^{2+} solution (1.1 ± 0.07 SE, n = 12) or treated with 100 nM ShK (1.06 ± 0.03 SE, n = 17). Resting Tem cells (day 6) had low levels of activated β1 integrin that were not significantly different ($p \geq 0.44$) than in control conditions (2 mM Ca^{2+};1.2 ± 0.04, SE, n = 4), 0 Ca^{2+} (1.2 ± 0.05, n = 4), or with ShK treatment (1.3 ±0.12, n = 4).

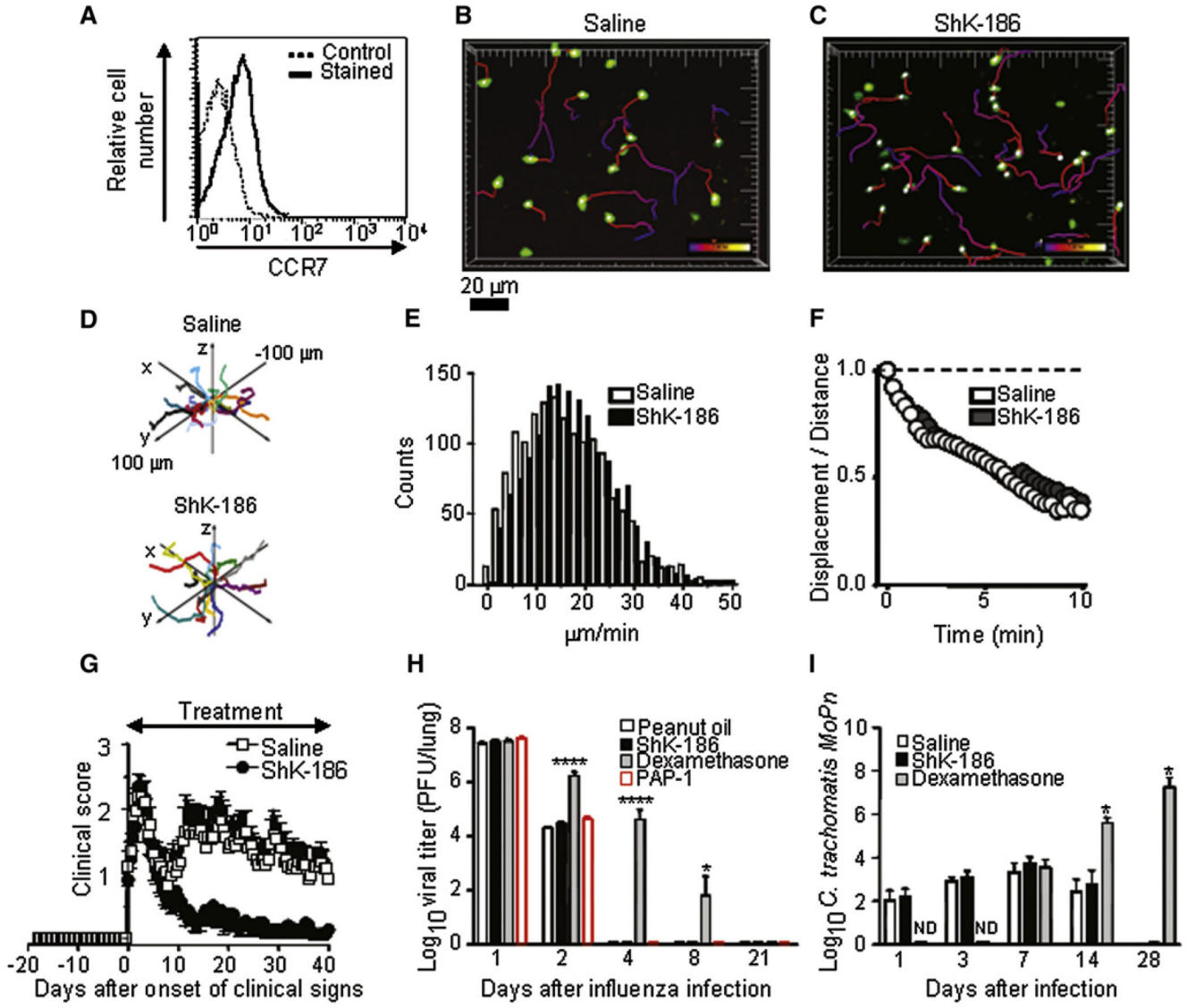

Figure 7. CCR7$^+$ T Cell Motility in the Lymph Node and Evaluation of Three Disease Models

(A) Adoptively transferred CD3$^+$ T cells are CCR7$^+$. Solid line = CCR7 staining; dotted line = background staining. The tissue-weight-normalized number of cells recovered from lymph nodes of saline- and ShK-186-treated animals did not differ, indicating no effect of ShK-186 treatment on homing to lymph node (data not shown, n = 2 for each condition).

(B and C) Images show maximum-intensity projection ''snapshots'' of CD3$^+$ CCR7$^+$ T cells in an inguinal lymph node 3 hr after treatment with saline or ShK-186 (100 μg/kg), respectively. Pseudocolored cell tracks depict T cell movements over 6 min.

(D) Representative 3D displacement plots of T cells in saline-treated (top) and ShK-186-treated lymph nodes (bottom) after normalizing starting coordinates.

(E) Distributions of instantaneous velocities of saline-treated (white) and ShK-186-treated (black) CD3$^+$ CCR7$^+$ T cells. Mean values (16.6 and 16.2 μm/min, respectively) are not statistically different.

(F) Meander index (displacement from origin/distance traveled) as a function of time for CCR7$^+$ T cells in lymph nodes from saline-treated (open circles) and ShK-186-treated animals (closed circles).

(G) Effect of ShK-186 on the course of CR-EAE. White, saline subcutaneous injection, n = 14 rats; black, ShK-186 100 μg/kg/day subcutaneous injection, n = 15 rats.
(H) Lack of effects of ShK-186 and PAP-1 on clearance of rat-adapted influenza virus. White, peanut oil orally, n = 5; red, PAP-1 50 mg/kg/day orally; black, ShK-186 100 μg/kg/day subcutaneous injection, n = 5 rats; gray, dexamethasone 2 mg/kg/day orally, n = 5. * $p < 0.05$, **** $p < 0.01$.
(I) Lack of effects of ShK-186 on clearance of *Chlamydia trachomatis*. White, saline subcutaneous injection, n = 10; black, ShK-186 100 μg/kg/day subcutaneous injection, n = 10; gray, dexamethasone 2 mg/kg/day subcutaneous injection, n = 4. Values were expressed as mean ± SD.